RADIATIVE PROPERTIES OF CIRRUS CLOUDS: FIRE IFO CASE 10/28/86

PAUL F. HEIN, WILLIAM L. SMITH, JR., AND STEPHEN K. COX

Department of Atmospheric Science, Colorado State University, Fort Collins, CO 80523

1. Data Analysis Procedures

A description of the radiative properties of two cirrus clouds sampled on 10/28/88 in the FIRE cirrus IFO is presented. The clouds are characterized in terms of the broadband infrared effective emittance, cloud fractional absorptance, shortwave (.3-2.8μ m) heating rate, cloud albedo and vertical velocity. The broadband fluxes used in these calculations were obtained from measurements made by pyranometers and pyrgeometers manufactured by Eppley Laboratories Inc. For a description of these radiometers and calibration procedures, see Albrecht and Cox (1976), Albrecht and Cox (1977) and Smith Jr. *et al.* (1988). In addition, the shortwave irradiances were corrected to a horizontal plane and normalized to the same time by taking into account Sabreliner flight information (i.e. pitch, roll, heading and angle of attack), as well as sun-earth geometry considerations (Ackerman and Cox, 1981; hereafter AC).

Since only one aircraft was used, broadband fluxes at different levels in the cloud were not measured simultaneously. As a result, sampling errors may occur due to the nonsteady state of the cloud field or due to the possibility that the flight legs were not flown directly above or below each other. To minimize these errors and to simplify the analysis, the necessary variables were averaged and the averages used in the calculations. The averaging for each flight leg was done in the following ways:

(1) Average the appropriate variables using every data point along a flight leg to determine a mean value for the cirrus cloud field.

(2) Average some percentage of the data to stratify the cloud into separate regimes (i.e. optically thicker or thinner than average).

The downwelling shortwave and longwave irradiances were used as selection criteria to remove cloud free data encountered along the data sampling leg.

(a) Shortwave Stratification

Find the lowest 30% of the downwelling shortwave irradiance values along each flight leg and average all irradiance variables corresponding to these points.

(b) Longwave stratification

Find the highest 30% of the downwelling longwave irradiance values along each flight leg and average all irradiance variables corresponding to these points.

The effective emittance (ϵ^*) is the ratio of the observed change in irradiance through a cloud layer to the change that would have occurred had the cloud been black. ϵ^*, as derived from the downward irradiance may defined as:

$$\epsilon^*(\downarrow) = \frac{H_B(\downarrow) - H_T(\downarrow)}{\sigma T_B^4 - H_T(\downarrow)}$$

where H( ) refers to the observed downwelling infrared irradiance, T is the mean temperature along the flight leg, the subscripts T and B refer to the top and bottom of the cloud layer, respectively, and σ is the Stefan Boltzman constant.

The cloud fractional absorptance (CFA) is described by AC and is defined as:

$$CFA = \frac{(H\downarrow - H\uparrow)_T - (H\downarrow - H\uparrow)_B - \sum_i H_{Si}}{H\downarrow_T},$$

where

$(H\downarrow - H\uparrow)_T \equiv$ net irradiance at cloud top,
$(H\downarrow - H\uparrow)_B \equiv$ net irradiance at cloud base,
$\sum_i H_{Si} \equiv$ net energy gain or loss through cloud sides (i.e., $\partial Hx/\partial x + \partial Hy/\partial y$),
$H\downarrow_T \equiv$ incoming irradiance at cloud top.

In seeking ways to quantitatively express the spatial variability of the observed variables, two techniques have been applied: a histogram analysis and a cumulative variance summary.

The histograms were created by applying thresholds to detrended data and calculating the size (in kilometers) of each section that exceeded the threshold. These sizes were then combined to form the histograms. In Figure 1,

an example graph, the +1 SD (standard deviation) threshold is exceeded between points F and G. The distance between F and G is then the size used in creating the histogram with the threshold of +1 SD. The count of the appropriate bin size will then be incremented. Similarly, the distance between E and H is the size used to increment the count of the appropriate bin for the +0.0 threshold. For the negative thresholds, -0.0 and -1 SD, the values must be less than the threshold (instead of being greater than for the positive thresholds) for the threshold to be exceeded. Thus, the section between points B and E, and the section between H and K, exceed the -0.0 threshold. Similarly, the section between points C and D, and the section between points I and J, exceed the -1 SD threshold. Sections of the graph at the ends of the data set that exceed a threshold (i.e. section to the left of point B for the +0.0 threshold) are not used because the size is unknown. Each histogram contains several different heights to increase the total number of sizes. Since the thresholds are based on standard deviations and not absolute values, the distribution of sizes at each height is expected to be similar.

The cumulative variance graphs were created by first using Fast Forrier Transforms to create a variance spectra. The variances were then summed in a cumulative fashion from the largest scalelengths (wavelengths) to the smallest. No detrending was done to the original data and no smoothing or averaging was done to the spectral points. Also, no points were removed due to the effect of the finite length of the file. This means that the spectral points at scalelengths larger than about 4000 m (especially greater than 8000 m) may only be qualitatively correct. The cumulative variance at the smaller scalelengths should be correct because a more accurate representation of the variance at the larger scalelengths should only redistribute the energy amongst the larger scalelengths.

2. Flight Description

The Sabreliner flight on the morning of 28 October 1986 was flown over the western shore of Lake Michigan. There was a shortwave (pressure) ridge over the region with a trough approaching from the west.

The cirrus, the Sabreliner flew through, was thin and had a banded structure. Cloud base of the upper cloud deck varied from about 8.8 km to 9.2 km with broken undercast beneath. Cloud top was at about 11.0 km.

The Sabreliner flew a racetrack pattern with the flight legs being oriented about 30 degrees off of the mean wind direction WNW. Because of the racetrack pattern, it became apparent that the cloud on the NW side had different characteristics than the cloud on the SE side of the racetrack. Therefore the data from each racetrack side were treated separately. "Cloud 1", on the SE side of the racetrack pattern, included the flight legs at heights: 11.3 km, 10.0 km, and 8.8 km. "Cloud 2", the NW side of the racetrack, was sampled at heights: 10.7 km, 9.4 km, and 8.5 km. Tables 1a and 1b show the times, positions and headings of the flight legs for each of the designated clouds.

Table 1a. Cloud 1 flight leg times, positions and headings.

Table 1a. Cloud 1 flight leg times, positions and headings.

Height (km)	Time (GMT)	Start Lat	Long	Time (GMT)	End Lat	Long	Heading
11.3	15:45:48	44.29	-87.89	15:48:58	44.45	-87.41	120
10.0	16:00:56	44.27	-87.89	16:04:31	44.45	-87.36	119
8.8	16:16:47	44.28	-87.93	16:20:41	44.44	-87.36	113

Table 1b. Cloud 2 flight leg times, positions and headings.

Table 1b. Cloud 2 flight leg times, positions and headings.

Height (km)	Time (GMT)	Start Lat	Long	Time (GMT)	End Lat	Long	Heading
10.6	15:36:22	44.37	-87.44	15:41:54	44.13	-88.14	292
10.7	15:53:20	44.86	-87.39	15:57:17	44.54	-87.91	288
9.4	16:07:45	44.65	-87.21	16:13:30	44.45	-87.93	289
8.5	16:24:44	44.52	-87.36	16:30:34	44.48	-88.11	275

3. Results

Cloud fractional absorptance values were deduced from pyranometer measurements in the .3-2.8 μ m spectral region with a correction made for sampling of finite cloud effects in the manner described by AC.

Figure 2 shows a plot of the solar cloud fractional absorptance vs the infrared emittance for the two, two layer cloud samples defined in Table 1. The lower values represent a layer with a 1.3 km geometric thickness while the higher values represent a 2.5 km thick layer. Values derived from both the SW stratification and the LW stratification are shown. As we mentioned above, the stratification of the data was necessary to eliminate the banded structure of cirrus cloud within each data leg. In essence, both clouds for both stratifications show very similar radiative properties with emittances between .48 and .55 for the thicker layers and .28 and .30 for the thinner layers; similarly the SW fractional absorptance varies from .08 to .09 for the thicker layers and .05 to .06 for the thinner layers. Within the errors of the observations, the slopes of the lines connecting these points

for the two clouds are essentially the same.

Layer SW heating rates for these same cloud layers are given in tables 2 and 3. The heating rates for the two layers are encouragingly similar as would be expected from the previous figure; for the top 1.3 km layer they vary between .23 and .29 ° C/hr and for the lower layer between .15 and .17 ° C/hr.

Figure 3 represents the SW reflectance observed at cloud top for Cloud 2 for three spectral bandpasses. This is an example of the structure of the observations in the raw data.

Figures 4 shows the results of the histogram analysis of scale size variation on the measured vertical velocity. It is notable that most of the vertical velocity "cells" have horizontal dimensions less than 3 km. Figure 5 shows that the downward visible irradiance shows essentially the same structure as the vertical velocity.

Figure 6 shows the cumulative variance analysis for the albedo at the top of cloud 2. The continuous line is a fit to the plotted data points. This graphs may be interpreted to show the per cent variance explained by scale lengths larger than a given value. For example, this figure suggests that 85% of the variance arises from features whose horizontal scale is greater than 10 km. Figure 7 illustrates the cumulative variance analysis for vertical velocity applied to each of the flight levels in the sample of cloud 2. The solid curve represents the 10.6 km height, the dashed curve - 9.4 km, and the dotted curve - 8.5 km. Notable is the narrowing of the scale length with increasing height. Fifty percent of the variance is explained by features larger than 13 km at the 10.6 km height, larger than 22 km at the 9.4 km level and larger than 50 km at the 8.5 km level.

4. Acknowledgements

This research has been supported by the National Science Foundation under Grant ATM-8521214 and by the National Aeronautics and Space Administration under Grant NAG 1-554.

REFERENCES

Ackerman, S. A., and S. K. Cox, 1981: Aircraft observations of the shortwave fractional absorptance of non-homogeneous clouds. *J. Appl. Meteor.*, **20**, 0128-0133.

Albrecht, B., and S. K. Cox, 1977: Procedures for improving pyrgeometer performance. *J. Appl. Meteor.*, **16**, 188-197.

Albrecht, B., and S. K. Cox, 1976: Radiation data reduction procedures for Sabreliner, C-130 and DC-6 aircraft during the GARP Atlantic Tropical Experiment. Colorado State University *Atmospheric Science Paper No. 244*, Fort Collins, CO., 100 pp.

Smith, Jr., W. L., S. K. Cox and V. Glover, 1988: Temperature sensitivity of Eppley broadband radiometers. Colorado State University *Atmospheric Science Paper No. 423*, Fort Collins, CO., 12 pp.

Table 2. Layer heating rates (.3-2.8 μm) in degrees/hr. for Cloud 1

	MEAN	IR STRATIFICATION	SW STRATIFICATION
Z = 11.3 Km			
	*	.233	.261
Z = 10.0 Km	*	(.216)	(.309)
	.171	.162	.173
Z = 8.8 Km	(.253)	(.263)	(.251)
	Values in parentheses uncorrected for cloud inhomogeneities		

*indicates heating rate indeterminate

Table 3. Layer heating rates (.3-2.8 μm) in degrees/hr. for Cloud 2

	MEAN	IR STRATIFICATION	SW STRATIFICATION
Z = 10.7 Km			
	*	.289	.266
Z = 9.4 Km	*	*	(.431)
	.128	.166	.148
Z = 8.5 Km	(.138)	(.181)	(.158)
	Values in parentheses uncorrected for cloud inhomogeneities		

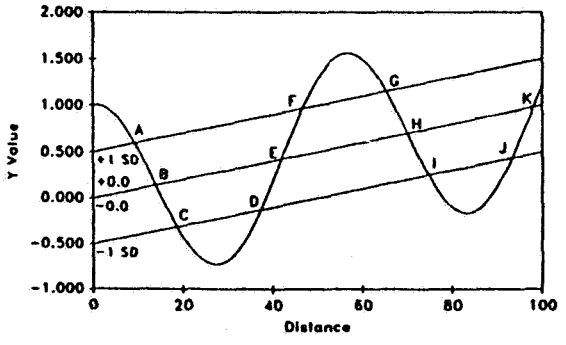

Figure 1. Example plot illustrating procedure for generation of size histogram plots (figs. 4 and 5).

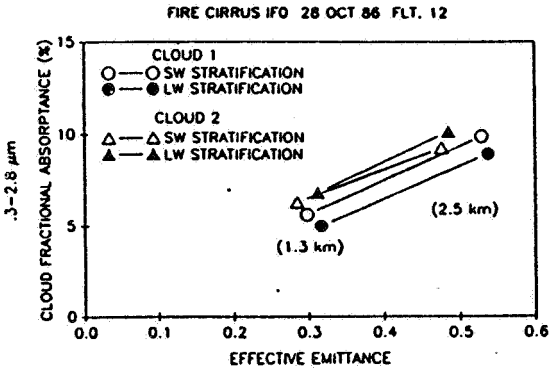

Figure 2. .3-2.8 μ m CFA vs. effective emittance for Cloud 1 and Cloud 2.

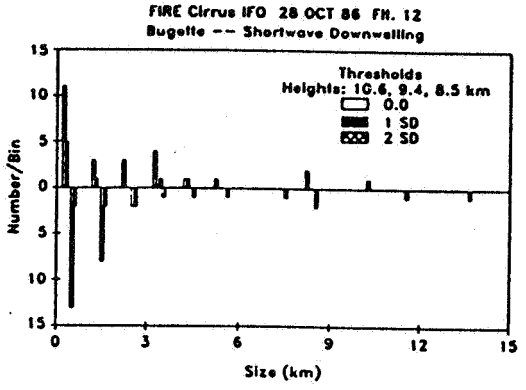

Figure 5. Same as Figure 4 but for downwelling shortwave irradiance.

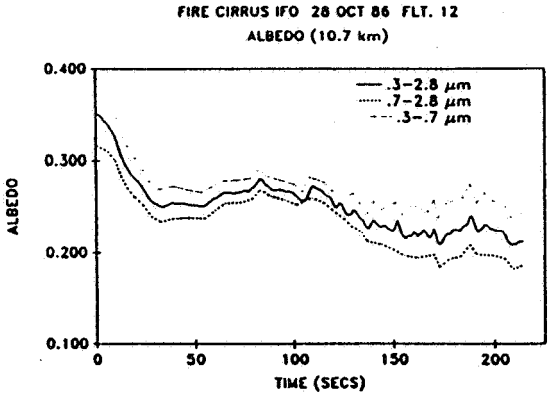

Figure 3. Albedo for Cirrus Cloud 2.

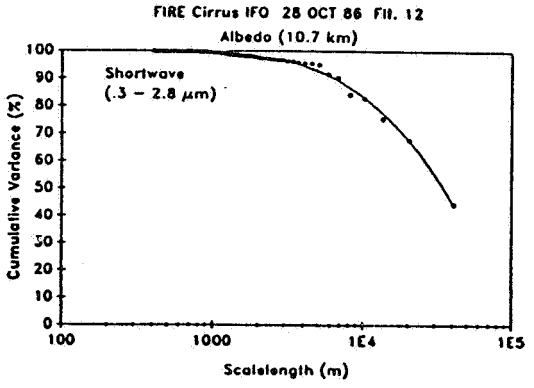

Figure 6. Cumulative variance of .3-2.8 μ m albedo for Cloud 2.

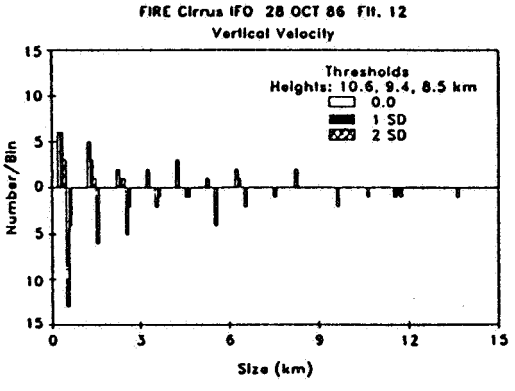

Figure 4. Histogram illustrating observed vertical velocity scale sizes (SD is standard deviation from detrended mean).

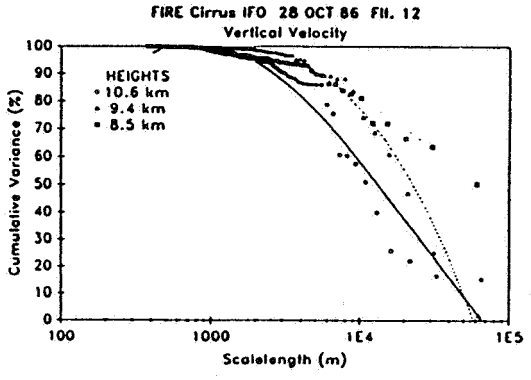

Figure 7. Cumulative variance of vertical velocity at different heights in Cloud 2.